Supplement of Atmos. Chem. Phys., 26, 9017–9036, 2026
https://doi.org/10.5194/acp-26-9017-2026-supplement

Atmospheric Chemistry and Physics
Open Access
EGU

Supplement of

Anthropogenic modulation of dust-dominated ice nucleation in an urban dryland city of China during winter and spring

Chengqing Chen et al.

Correspondence to: Yang Wang (wang_yang@lzu.edu.cn)

Contents

S1. Definition and Calculation Methods of Normalized Ice Nucleation Parameters

In this study, to systematically evaluate the ice-nucleating ability of different aerosol components, we employed multiple normalization methods to characterize ice nucleation activity (Moore et al., 2025). The activation fractions $N_{D>0.5}$ and $N_{D>1.0}$ represent the observed INPs concentration normalized to the number concentration of aerosol particles with diameters greater than 0.5 μm ($n_{0.5}$) and 1 μm ($n_{1.0}$), both constrained to particles smaller than 2.5 μm. respectively. Their corresponding equations are provided as Eq.(S1) and Eq.(S2). In addition, a normalization parameter based on the total aerosol surface area (SAtot), denoted as N_s, was used. Its calculation method is shown in Eq. (S3). This indicator reflects the nucleation potential per unit surface area.

$$N_{\mathrm{D>0.5}}(\mathrm{T}) = \frac{N_{\mathrm{INP}}(\mathrm{T})}{n_{0.5}} \tag{S1}$$

$$N_{\mathrm{D>1.0}}(\mathrm{T}) = \frac{N_{\mathrm{INP}}(\mathrm{T})}{n_{1.0}} \tag{S2}$$

$$N_{\mathrm{s}}(\mathrm{T}) = \frac{N_{\mathrm{INP}}(\mathrm{T})}{SA_{\mathrm{tot}}} \tag{S3}$$

S2. Definition and modification of the sensitivity metric A^{-1}

A sensitivity metric $A_{\mathrm{dust,lab}}$ to quantify the relative importance of temperature and dust abundance for immersion freezing (Villanueva et al., 2025). Based on laboratory constraints, INP concentrations were expressed as a function of the logarithm of dust aerosol optical depth (LD) and temperature (T):

$$\mathrm{INP_{dust}(T,LD)} = \mathrm{C_1 \cdot LD \cdot exp(-}A_{\mathrm{dust,lab}}\,\mathrm{T)} \tag{S4}$$

where $A_{\mathrm{dust,lab}}$ ($\mathrm{K^{-1}}$) is the slope parameter governing temperature sensitivity. By definition, as shown in Eq.(S5).

$$A_{\mathrm{dust,lab}} = \frac{\left(\frac{\partial \mathrm{INP}}{\partial \mathrm{T}}\right)}{\left(\frac{\partial \mathrm{INP}}{\partial \mathrm{LD}}\right)} \tag{S5}$$

In our observational framework, we adapt this metric to surface measurements by replacing dust aerosol optical depth (DAOD) with Fine mineral dust (FMD) mass concentration as a robust proxy for mineral dust. In addition, secondary inorganic aerosol (SNA) is included as a marker of secondary aerosols, allowing us to assess how pollution modulates the dust-temperature sensitivity balance. Specifically, we

employ the following log-linear regression model:

$$\ln(\mathrm{INP}) = b_0 + b_1 \ln(\mathrm{FMD}) + b_2\,(-\mathrm{T}) + b_3 \ln(\mathrm{SNA}) + b_4\,[\ln(FMD)\ln(SNA)] + \varepsilon \qquad \text{(S6)}$$

where b_1 represents the main effect of FMD, b_2 the temperature sensitivity, b_3 the main effect of SNA, and b_4 the FMD–SNA interaction term. The term ε denotes the residual error.

From this regression model, the dust sensitivity conditional on SNA is given by:

$$\frac{\partial \ln(\mathrm{INP})}{\partial \ln(\mathrm{FMD})} = b_1 + b_4\, z, \quad z = \ln(\mathrm{SNA}) \qquad \text{(S7)}$$

while the temperature sensitivity is:

$$\frac{\partial \ln(\mathrm{INP})}{\partial(-\mathrm{T})} = b_2 \qquad \text{(S8)}$$

Accordingly, we define the observational A and A^{-1} as:

$$\mathrm{A(z)} = \frac{b_2}{b_1 + b_4\, z} \text{ and } \mathrm{A^{-1}(z)} = \frac{b_1 + b_4\, z}{b_2} \qquad \text{(S9)}$$

where A ($\mathrm{K^{-1}}$) denotes the number of "e-fold dust increases" equivalent to 1 K cooling, and A^{-1} ($\mathrm{K^{-1}}$) denotes the effective cooling equivalent to one e-fold (i.e., based on the natural exponential e) dust increase.

S3. Empirical parameterization schemes for INPs

To quantitatively describe the relationship between INP concentrations, temperature, and aerosol properties, we constructed two empirical parameterization models.

Following the exponential form of Meyers et al. (1992), a single-parameter model was established with air temperature (T, in K) as the sole predictor (Eq.(S10)):

$$N_{\mathrm{IN,T_k}} = \exp[a_1 + b_1\,(273.15 - \mathrm{T_k})] \qquad \text{(S10)}$$

where a_1 and b_1 are regression coefficients fitted to the observed dataset. The second scheme adopts the framework of DeMott et al. (2010), which originally incorporated $n_{0.5}$ together with temperature. In this study, we modified the predictor to $n_{1.0}$, in order to better represent coarse-mode aerosols observed in Lanzhou, and re-fitted all coefficients using the measurement dataset (Eq.(S11)):

$$\mathrm{n_{IN,T_k}} = \mathrm{a_2}(273.16 - \mathrm{T_k})^{\mathrm{b_2}}(\mathrm{n_{1.0}})(\mathrm{c_2}(273.16 - \mathrm{T_k}) + \mathrm{d_2}) \qquad \text{(S11)}$$

where a_2, b_2, c_2, d_2 are empirical fitting parameters.

S4. Calculation Equation for ice nucleation activity evaluation index

To evaluate the fitting accuracy of INP parameterization, this study used three statistical metrics: coefficient of determination (R^2), root-mean-square error (RMSE), and fraction of predictions within a factor of 5 (FAC_5). The formulas are provided in Eq.(S12–14). All metrics are computed in the natural log space (ln) to mitigate the influence of data with different orders of magnitude on the statistical results.

$$R^2 = 1 - \frac{\sum_{i=1}^{n}\left[\ln\left(N_{\mathrm{obs},i}\right) - \ln\left(N_{\mathrm{fit},i}\right)\right]^2}{\sum_{i=1}^{n}\left[\ln\left(N_{\mathrm{obs},i}\right) - \overline{\ln(N_{\mathrm{obs}})}\right]^2} \tag{S12}$$

$$\mathrm{RMSE} = \sqrt{\frac{1}{n}\sum_{i=1}^{n}\left[\ln\left(N_{\mathrm{obs},i}\right) - \ln\left(N_{\mathrm{fit},i}\right)\right]^2} \tag{S13}$$

$$\mathrm{FAC_5} = \frac{1}{n}\sum_{i=1}^{n}\left[\left|\ln\left(N_{\mathrm{fit},i}\right) - \ln\left(N_{\mathrm{obs},i}\right)\right| \le \ln(5)\right] \times 100\% \tag{S14}$$

Here, $N_{\mathrm{obs,i}}$ and $N_{\mathrm{fit,i}}$ represent the observed and predicted INP concentrations, respectively. The variable n is the sample size.

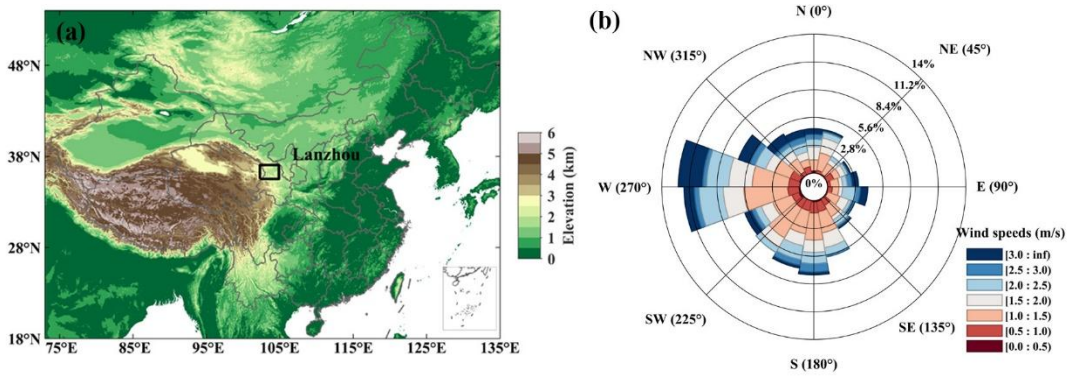

74

75 Fig. S1. Geographical location of Lanzhou City and wind characteristics during the observation period. (a)
76 Geographical location and topography of Lanzhou City in northwestern China. The black rectangle indicates the
77 study region. (b) Wind rose showing the distribution of wind direction and wind speed.

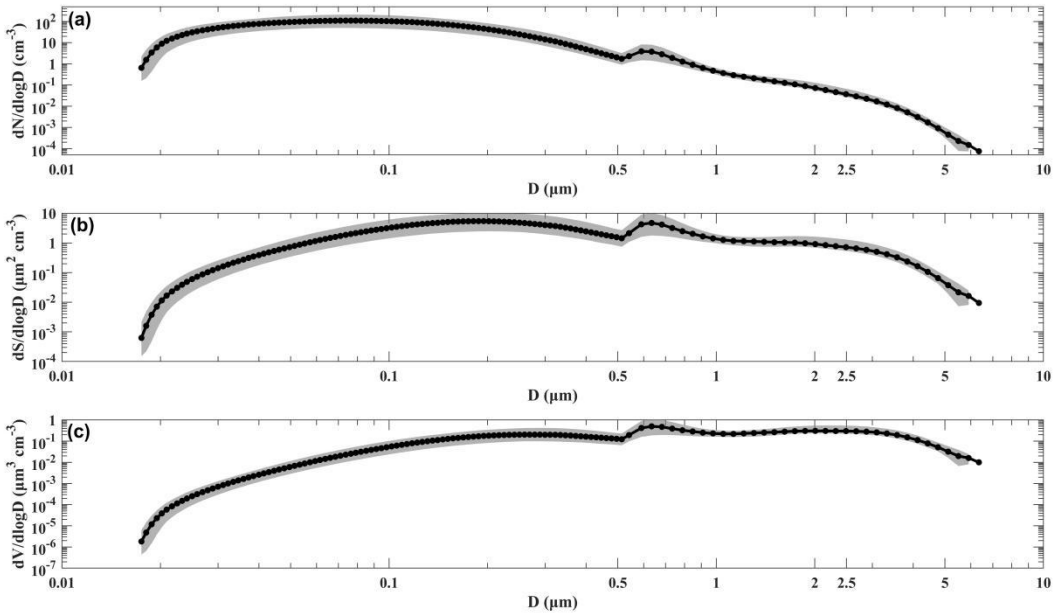

78

79 Fig. S2. Aerosol Size Distribution Characteristics. (a) Particle Number Density Distribution. (b) Surface Area
80 Density Distribution. (c) Volume Density Distribution. The black solid circles represent the median for all time
81 periods in each particle size range, and the grey shading denotes the range between the 25th and 75th percentiles.

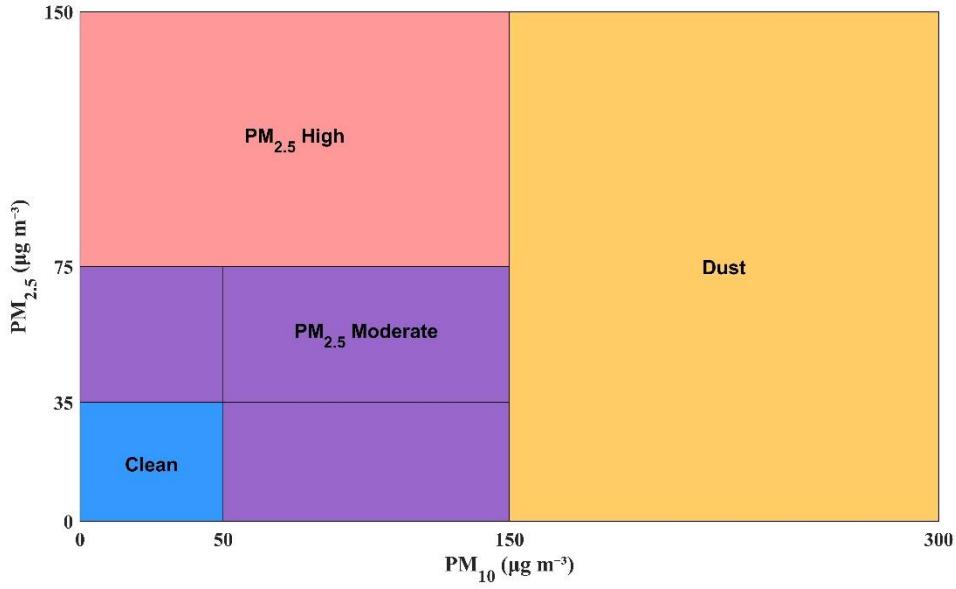

Fig. S3. Aerosol type classification based on PM_{10} and $PM_{2.5}$ concentrations. Four categories are defined using threshold values of $PM_{2.5}$ (35, 75 μg m^{-3}) and PM_{10} (50, 150 μg m^{-3}), following the Chinese National Ambient Air Quality Standards (GB3095-2012).

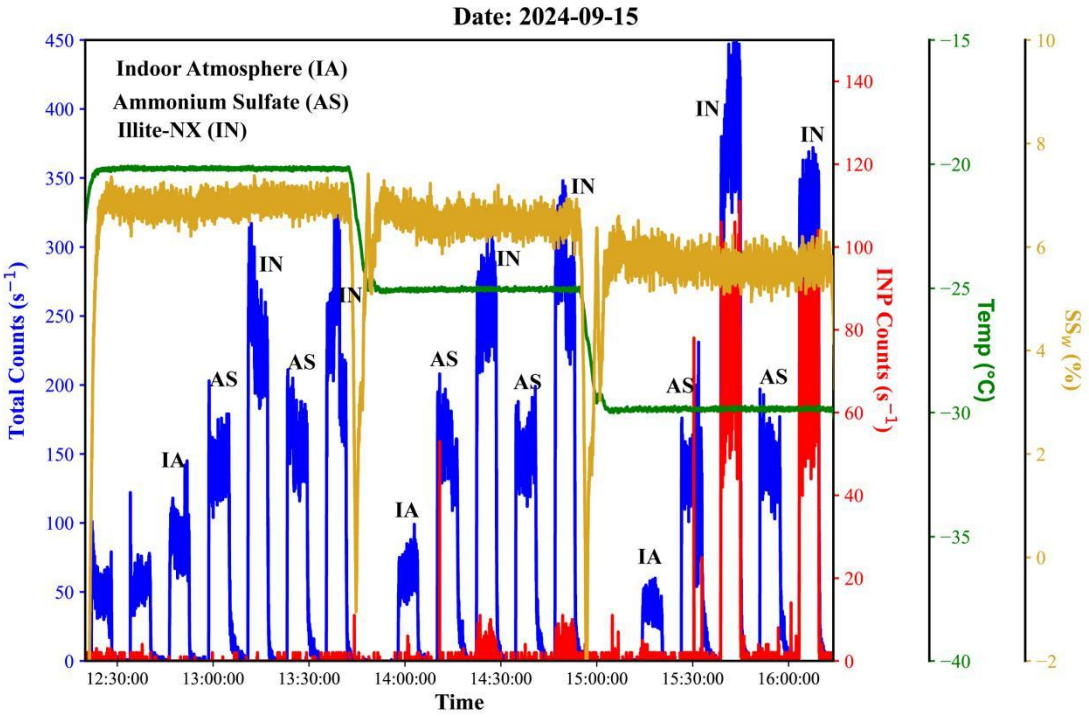

Fig. S4. Aerosol ice nucleation activity tests performed at different temperatures under identical supersaturation conditions. Indoor atmospheric samples, ammonium sulfate, and illite-NX were tested separately for their ice nucleation activity. The figure presents time series at one-second resolution for total particle count, INPs count, temperature, and supersaturation relative to water (SS_w).

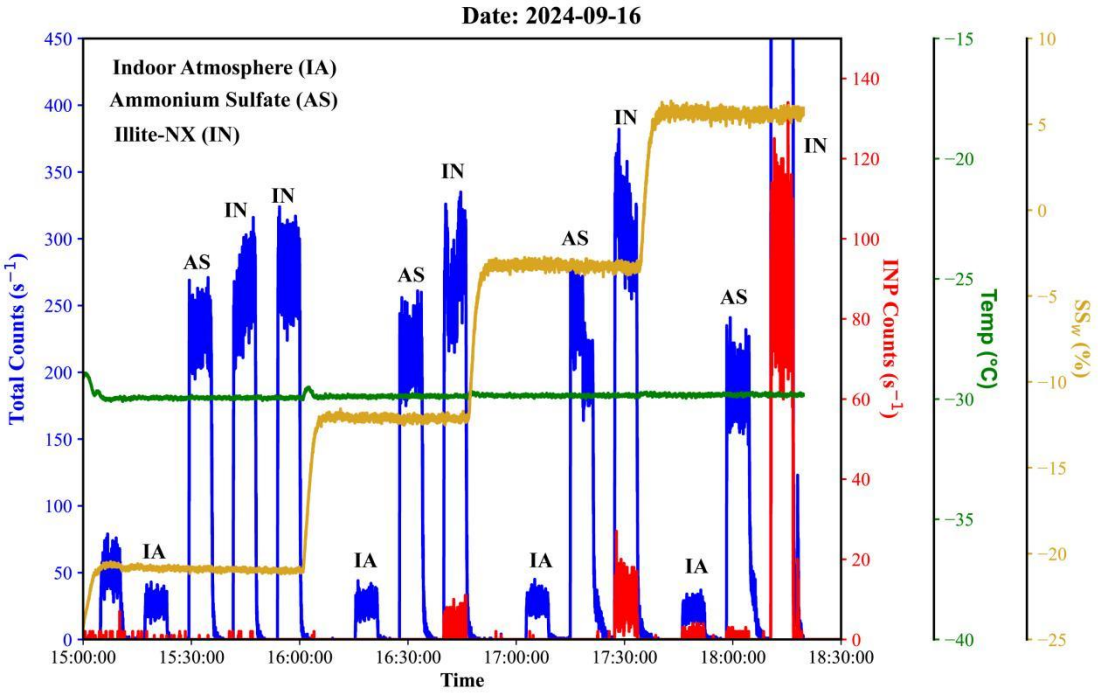

Fig. S5. Ice nucleation activity test of aerosol particles under different supersaturation conditions at a constant temperature. Indoor atmospheric samples, ammonium sulfate, and illite-NX were tested separately for their ice nucleation activity. The figure presents time series at one-second resolution for total particle count, INPs count, temperature, and supersaturation relative to water (SS_w) .

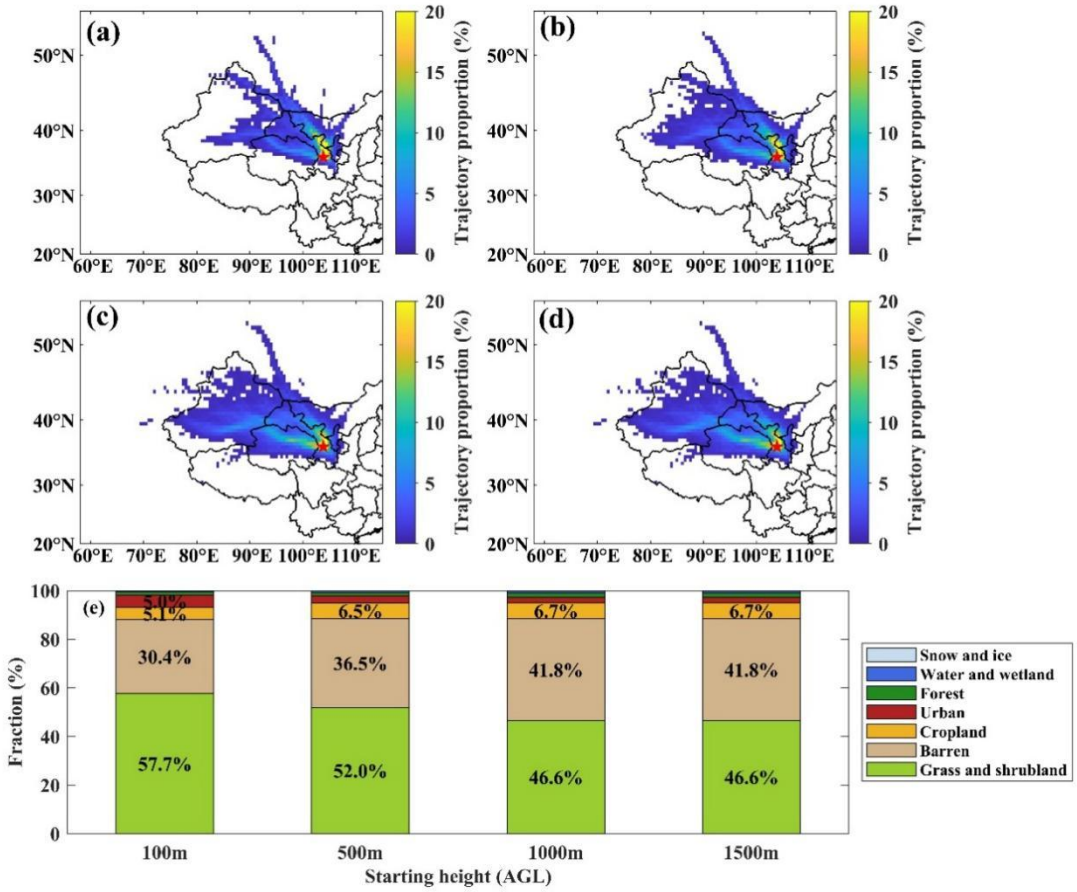

Fig. S6. Source regions and land-cover characteristics of backward trajectories arriving in Lanzhou. Spatial distributions of 72-h backward trajectory frequencies (trajectory proportion, %) for air masses arriving at Lanzhou at four starting heights above ground level (AGL): (a) 100 m, (b) 500 m, (c) 1000 m, and (d) 1500 m. The red star indicates the sampling site. Panel (e) shows the fractional contributions of major land-cover types sampled by the trajectories at the corresponding starting heights, including snow and ice, water and wetland, forest, urban, cropland, barren, and grass and shrubland.

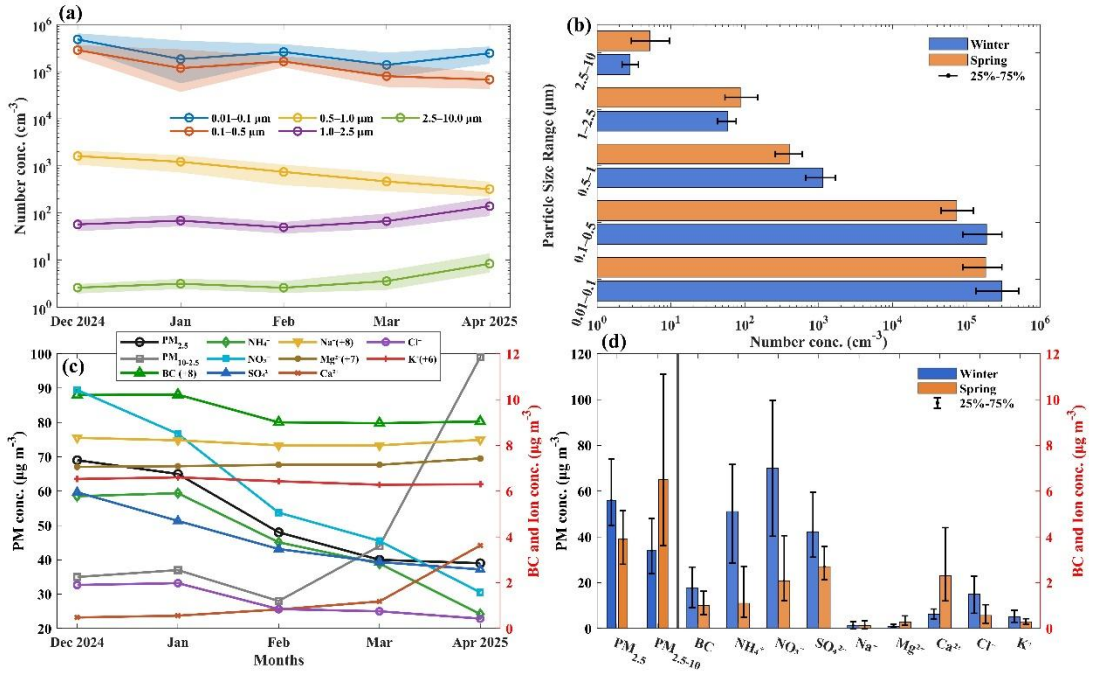

Fig. S7. Monthly variations and Seasonal differences in aerosol size distribution, PM mass concentrations, and water-soluble ion components. (a) Monthly median aerosol number concentrations in five size bins. (b) Seasonal median aerosol number size distributions. (c) Monthly median mass concentrations. Values in parentheses denote the offsets applied for graphical clarity and actual concentrations should be obtained by subtracting the offset values. (d) Seasonal mass concentrations of the same species as in (c). Unless otherwise noted, error bars and shaded areas represent the 25th–75th percentile ranges.

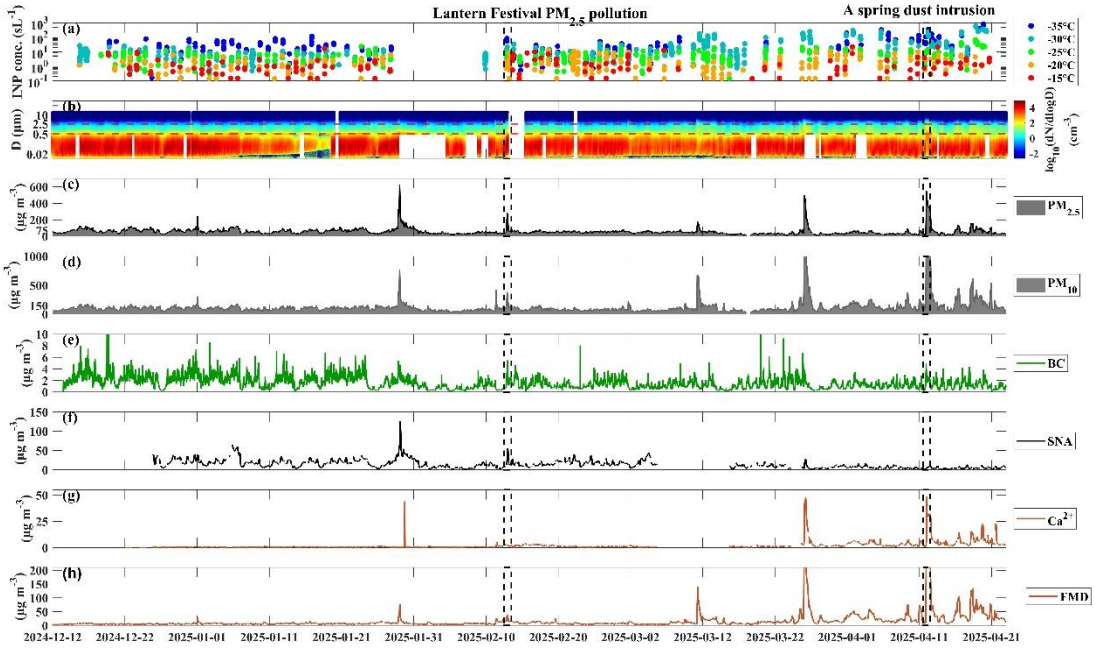

Fig. S8. Time series of INPs and aerosol characteristics. (a) INP concentrations at five activation temperatures. (b) Aerosol particle size distribution. The red dashed lines indicate particle sizes of 0.5 μm and 2.5 μm. Data gaps are shown as blank areas. (c)–(h) Time series of $PM_{2.5}$, PM_{10}, BC, SNA, water-soluble Ca^{2+}, and FMD, respectively. Vertical dashed lines denote representative aerosol events analyzed in Sect. 3.1.

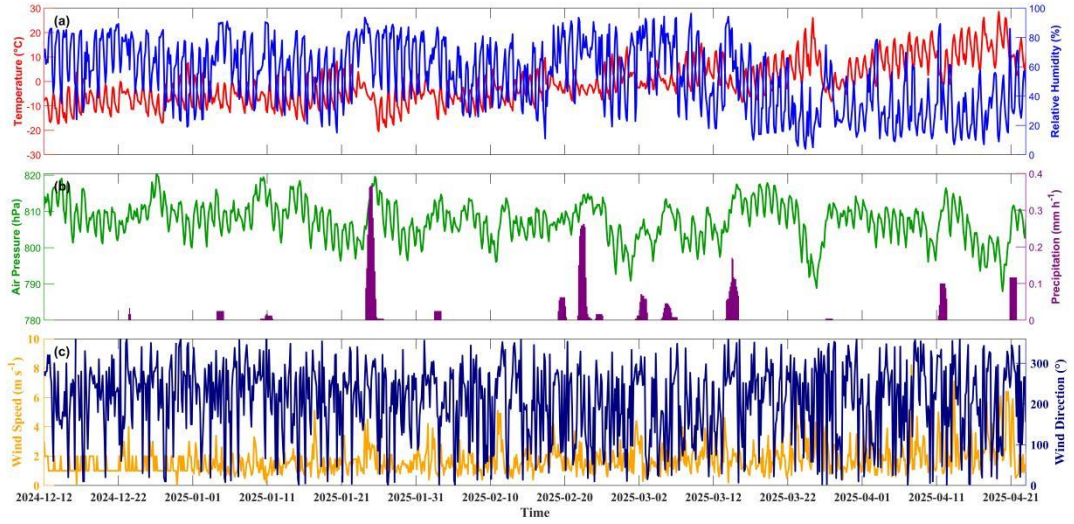

Fig. S9. Time series of key meteorological variables at the Yuzhong meteorological station. (a) Temperature and relative humidity. (b) Air pressure and precipitation. (c) Wind speed and direction. The station is located approximately 30 km from the sampling site. Data source: NOAA National Centers for Environmental Information, Global Surface Hourly Data for Station 529830-99999 (Yuzhong), China, 2010–2020; accessed June 1, 2025.

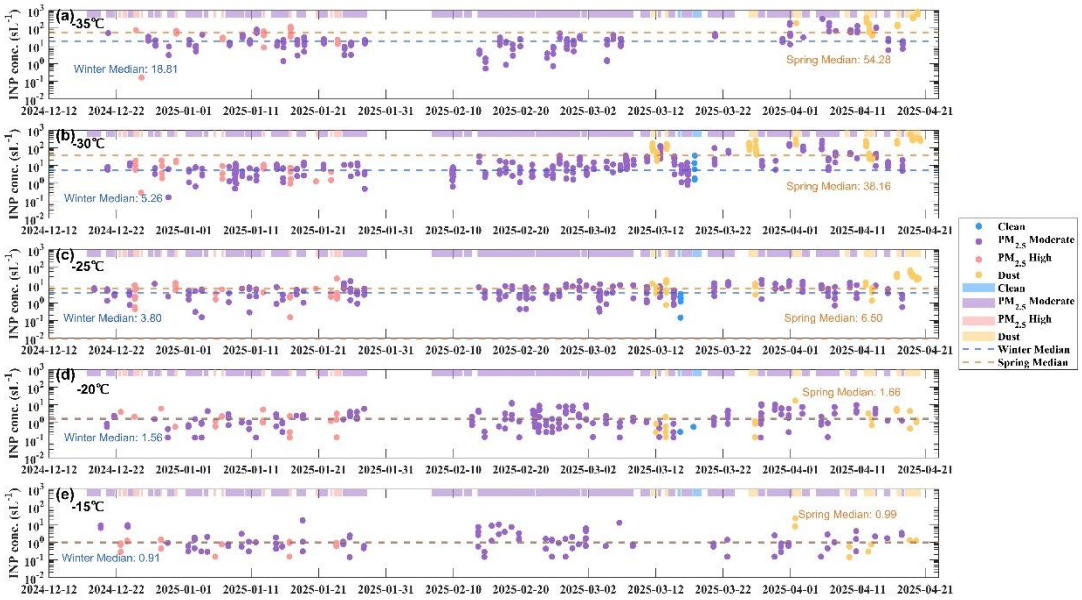

Fig. S10. Time series of INP concentrations at different temperature layers. The shaded areas in distinct colors represent the temporal distribution of different aerosol types, with the INP concentration for each aerosol type indicated by scattered points of corresponding colors. The dotted line indicates the median INP concentration for all aerosol types in winter and spring, with the values shown in the corresponding colors.

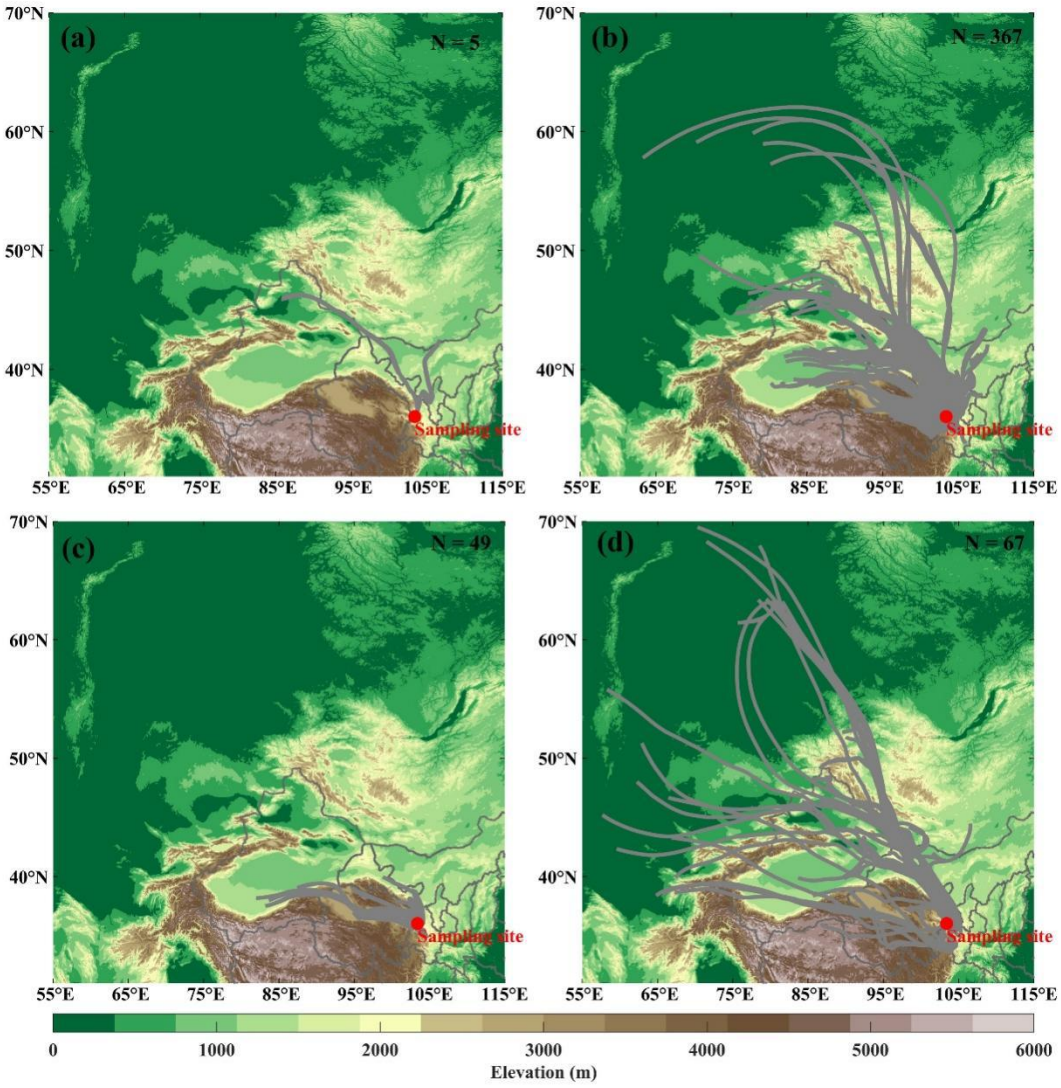

125

126 Fig. S11. 72-hour backward trajectory distribution of different aerosol event types. (a) Clean events. (b) $PM_{2.5}$
127 Moderate events. (c) $PM_{2.5}$ High events. (b) Dust events. The gray curve shows a single backward trajectory for the
128 event type, with the starting point located at an altitude of 100 m at the sampling site. The number of trajectories (N)
129 for the event type is shown in the upper right corner.

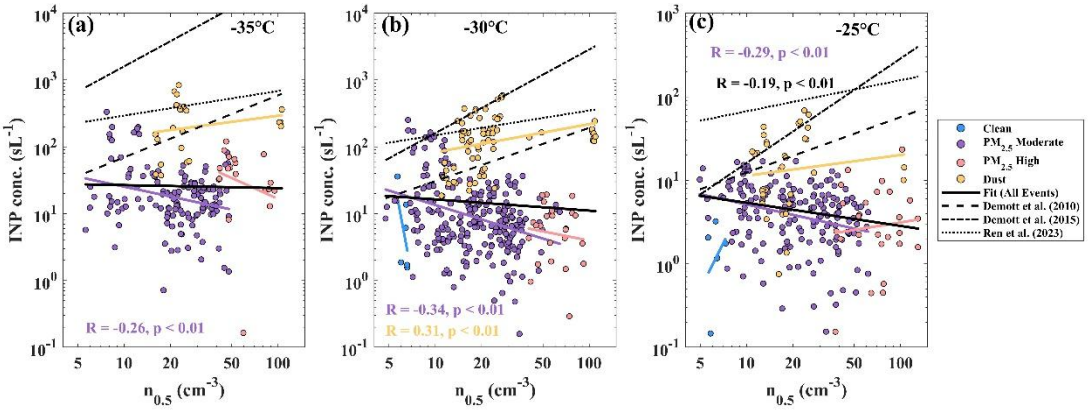

130

131 Fig. S12. Relationships between INPs and aerosol number concentrations. (a–c) show the relationships between INP

concentrations and $n_{0.5}$. The black dashed line indicates the prediction from existing parameterization schemes. The R and p values represent the Pearson correlation coefficient and its significance, and only results with $p < 0.01$ are shown.

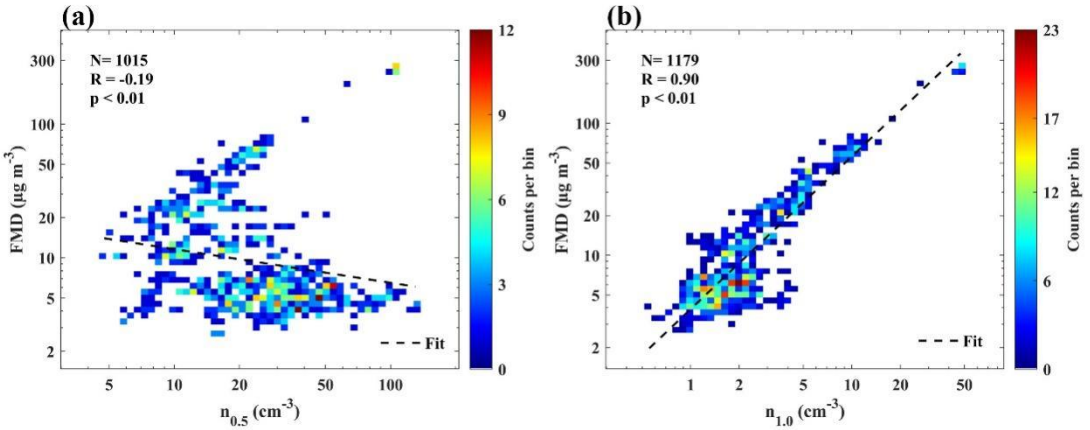

Fig. S13. Relationships between FMD and aerosol number concentrations. Two-dimensional histograms of $n_{0.5}$ and $n_{1.0}$ versus PMD, respectively. Data from five temperatures and four aerosol event types are combined. The X and Y axes are binned into 50 intervals in the natural log space, and the color shading indicates the number of samples in each bin. N denotes the total number of data points. R and p are the Pearson correlation coefficient and the corresponding significance level.

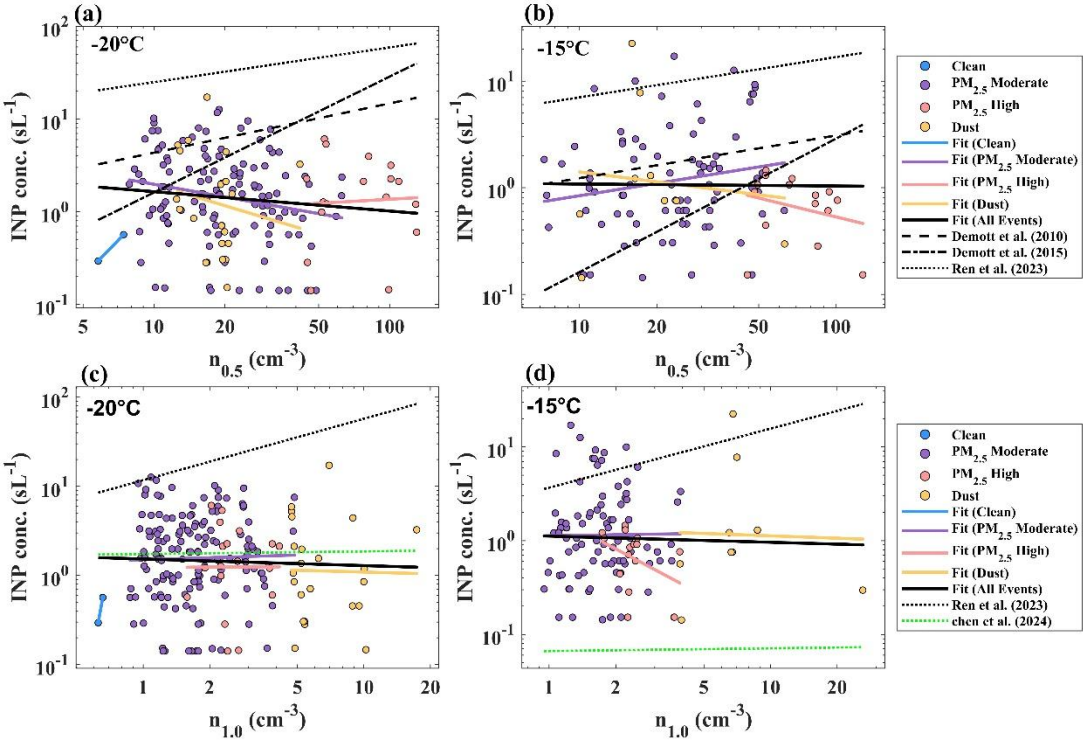

Fig. S14. Relationships between INP concentration and aerosol number concentrations. (a–b) show the relationships between INP concentration and $n_{0.5}$, while (c–d) depict the relationships with $n_{1.0}$. The R and p values represent the Pearson correlation coefficient and its significance, and only results with $p < 0.01$ are shown. The black solid line shows the fit for all samples, and the black dashed line indicates the prediction from existing parameterization schemes.

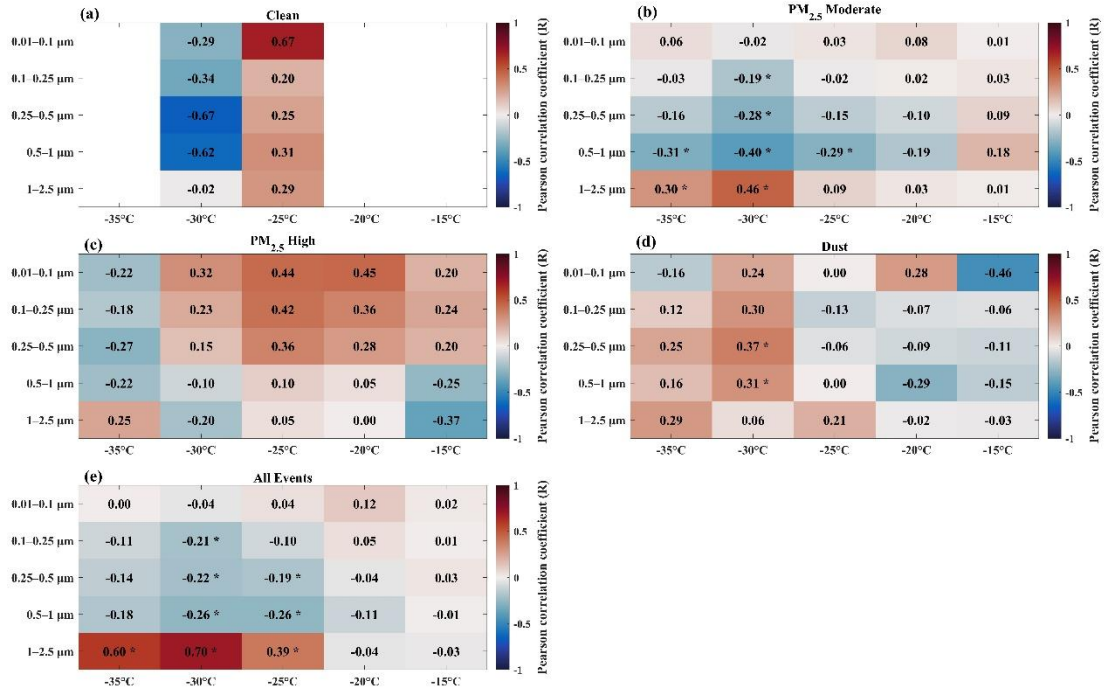

Fig. S15. Pearson correlations between INP concentrations and aerosol particle number concentrations across different event types. The *R* represent the Pearson correlation coefficient, calculated in the natural log space. Statistically significant correlations ($p < 0.01$) are marked with asterisks.

Table S1. Monthly and seasonal (winter and spring) median concentrations and interquartile ranges (25th–75th percentiles) of crustal trace metals (Ca, Al, Si, Fe, and Ti)

Time period	Ca	Al	Si	Fe	Ti
2024-12	322.65 (249.84–405.14)	804.00 (736.00–900.00)	493.37 (415.97–569.82)	475.54 (261.04–820.95)	14.20 (11.60–17.13)
2025-01	444.36 (321.61–574.20)	852.00 (759.00–984.00)	701.63 (576.73–910.34)	640.27 (418.96–1029.76)	22.32 (17.48–32.70)
2025-02	541.77 (355.66–842.28)	852.00 (748.00–1000.00)	927.83 (630.40–1531.80)	448.66 (302.50–700.91)	25.54 (18.70–37.85)
2025-03	1069.35 (500.68–1585.91)	1048.00 (820.00–1354.00)	1976.93 (897.48–3044.36)	681.28 (352.56–1158.29)	46.50 (23.32–69.65)
2025-04	2644.23 (1544.39–4610.21)	1824.50 (1284.00–2593.00)	5195.02 (2780.97–8903.08)	1538.75 (899.98–2450.60)	111.91 (63.53–185.18)
Winter	421.98 (297.78–580.78)	836.00 (748.00–956.00)	667.39 (491.08–957.53)	529.55 (327.93–838.15)	20.24 (14.61–28.98)
Spring	1507.89 (895.95–2870.87)	1280.00 (972.00–1946.00)	2746.33 (1713.39–5838.72)	964.06 (571.82–1781.12)	62.10 (40.41–123.53)

Note: Concentrations are in ng m^{-3}. Data span from 12 December 2024 to 20 April 2025.

Table S2. Fitting results of single-parameter INPs models under different pollution event types

Event	a_1	b_1	R^2	RMSE	FAC_5
All Event	-3.0599	0.1875	0.39	1.40	76.33%
Clean	-6.2371	0.2597	0.44	1.06	84.62%
$PM_{2.5}$ Moderate	-2.3477	0.1492	0.41	1.11	84.98%
$PM_{2.5}$ High	-3.2722	0.1746	0.49	1.15	86.54%
Dust	-6.0673	0.3531	0.70	1.11	89.20%

Table S3. Fitting results of two-parameter models for INPs concentration prediction in Lanzhou

a_2	b_2	c_2	d_2	R^2	RMSE	FAC_5
0.0007	2.6168	0.0934	-1.6206	0. 59	1.15	82.78%

157

158 Chen, J., Wu, Z., Gong, X., Qiu, Y., Chen, S., Zeng, L., and Hu, M.: Anthropogenic dust as a significant
159 source of ice-nucleating particles in the urban environment, Earth's Future, 12, e2023EF003738,
160 doi:10.1029/2023EF003738, 2024.
161 DeMott, P. J., Prenni, A. J., Liu, X., Kreidenweis, S. M., Petters, M. D., Twohy, C. H., Richardson, M.
162 S., Eidhammer, T., and Rogers, D. C.: Predicting global atmospheric ice nuclei distributions and their
163 impacts on climate, Proc. Natl. Acad. Sci. U.S.A., 107, 11217–11222, doi:10.1073/pnas.0910818107,
164 2010.
165 DeMott, P. J., Prenni, A. J., McMeeking, G. R., Sullivan, R. C., Petters, M. D., Tobo, Y., Niemand, M.,
166 Möhler, O., Snider, J. R., Wang, Z., and Kreidenweis, S. M.: Integrating laboratory and field data to
167 quantify the immersion freezing ice nucleation activity of mineral dust particles, Atmos. Chem. Phys.,
168 15, 393–409, doi:10.5194/acp-15-393-2015, 2015.
169 Meyers, M. P., DeMott, P. J., and Cotton, W. R.: New primary ice nucleation parameterizations in an
170 explicit cloud model, J. Appl. Meteorol., 31, 708–721, doi:10.1175/1520-
171 0450(1992)031<0708:NPINPI>2.0.CO;2, 1992.
172 Moore, K. A., Hill, T. C. J., Madawala, C. K., Leibensperger III, R. J., Greeney, S., Cappa, C. D., Stokes,
173 M. D., Deane, G. B., Lee, C., Tivanski, A. V., Prather, K. A., and DeMott, P. J.: Wind-driven emission
174 of marine ice-nucleating particles in the Scripps Ocean-Atmosphere Research Simulator (SOARS),
175 Atmos. Chem. Phys., 25, 3131–3159, https://doi.org/10.5194/acp-25-3131-2025, 2025.
176 Ren, Y. Z., Bi, K., Fu, S. Z., Tian, P., Huang, M. Y., Zhu, R. H., and Xue, H. W.: The relationship of
177 aerosol properties and ice-nucleating particle concentrations in Beijing, J. Geophys. Res. Atmos., 128,
178 e2022JD037383, doi:10.1029/2022JD037383, 2023.
179 Villanueva, D., Stengel, M., Hoose, C., Bruno, O., Jeggle, K., Ansmann, A., and Lohmann, U.: Dust-
180 driven droplet freezing explains cloud-top phase in the Northern Extratropics, Science, 389, 521–525,
181 doi:10.1126/science.adt5354, 2025.